Fracture Geometry and Statistics of Ceres' Floor Fractures

K. Krohn[1], D. L. Buczkowski[2], I. von der Gathen[1], R. Jaumann[1,3], F. Schulzeck[1], K. Stephan[1], R. Wagner[1], J. E. C. Scully[4], C. A. Raymond[4], C. T. Russell[5]

[1]Institute of Planetary Research, German Aerospace Center, Berlin, Germany; [2]Johns Hopkins University Applied Physics Laboratory, Laurel, MD, USA; [3]Freie Universiät Berlin, Germany; [4]NASA JPL, California Institute of Technology, Pasadena, California, USA; [5]UCLA, Institute of Geophysics, Los Angeles, CA, USA

Corresponding author: Katrin Krohn, katrin.krohn@dlr.de, Rutherfordstraße 2, 12489 Berlin, Germany

Keywords: Ceres, dwarf planet, floor fractured craters

Highlights:

- We measured 2336 fractures in thirteen floor-fractured craters (FFC) on Ceres.
- Floor-fractured craters on Ceres share similarities with FFCs on other planetary bodies especially those on the Moon and Mars.
- On Ceres some floor-fractured craters are impact-driven; other appear to be related to cooling-melting processes, outgassing and/or tectonics such as doming of the subsurface.
- Fracture studies point out brittle surface materials.

Abstract

Floor-fractured craters are one of the most distinct features on Ceres. Most of the fractures are located on the crater floors. The floor-fractures are concentric, radial or polygonal and share similarities with Class 1 and 4 floor-fractured craters (FFC) on the Moon (e.g., Buczkowski et al., 2018; Schultz, 1976) In total we measured 2336 fractures in thirteen craters. We analyzed their width, length, orientation and density.

Floor-fractures on Ceres do not show a global uniform sense of orientation. Nevertheless, two or more preferred orientations can be found in nearly every crater. The density map illustrates that there is typically no decrease of fracturing from the crater center to the crater rim and denotes formation mechanisms that are not necessarily impact driven. Because of the variation in these parameters, it is more likely that FFC on Ceres are globally independent and show different formation mechanisms. The geometry of the floor-fractures suggests an inhomogeneous, brittle surface material, in some cases with volatile components. We also propose that mechanisms on Ceres are especially comparable to those on the Moon and Mars. Additionally, these also include cooling/melting processes, degassing, and subsidence of the crater floor by up-doming of subsurface material as a result of absolute tensile stresses.

1 Introduction

In 2015, NASA's spacecraft Dawn reached the orbit of Ceres, its second destination after the asteroid Vesta, both are the two most massive objects in the asteroid belt. Aim of this mission was the interest in the composition and evolution of the bodies to draw conclusions concerning the history of the early solar system (McCord and Sotin, 2005; Russell and Raymond, 2011; Russell et al., 2016). Therefore, three instruments are onboard the spacecraft: the Framing Camera (FC) (Sierks et al., 2011), a Visible and Infrared Spectrometer (VIR) (De Sanctis et al., 2011) and a Gamma Ray and Neutron Detector (GRaND) (Prettyman et al., 2011). Based on the data provided by these instruments, Ceres' surface appears to consist of a differentiated rock or rock-ice mixture with constituents such as phyllosilicates (ammoniated, Mg- and Na- bearing), carbonates and dark material (Ammannito et al., 2016; Castillo-Rogez and McCord, 2010; De Sanctis et al., 2015; Park et al., 2016) spread over the body. Small quantities of H_2O-ice are also visible in a few locations (Combe et al., 2016).

Structures that emboss Ceres' surface are craters with a high variation in morphology, size and habitus. One peculiar crater type comprises polygonal shape (Otto et al., 2016), some other are modified by terraces, slides and flow features. Central peaks or pits, fractures or smooth terrains are also distinct in these craters (Buczkowski et al., 2016). Linear features, such as Samhain Catenae and small crater chains are other prominent features (Buczkowski et al., 2016).

The craters we focus on in this paper are those, which exhibit cracks on their crater floors. In the literature they are known as floor-fractured craters (FFC). Floor-fractured craters are one of the most distinct surface features on Ceres and are comparable to those on other planetary bodies like the Moon, Mars, Venus, Mercury or icy satellites (Buczkowski et al., 2016; Buczkowski et al., 2018;

Korteniemi et al., 2006; von der Gathen et al., 2016; Wichman and Schultz, 1995b). Schultz (1976) defined six different FFC classes subject to their morphological diversities for craters on the Moon. Lunar Class I craters are those with deep floors, central peak complexes, wall slumps and hummocky ejecta blankets. Their fractures are concentric, radial, and/or polygonal. Typical for Class IV craters are a wide and flat moat structure adjacent around the crater wall (Jozwiak et al., 2012; Schultz, 1976). These classifications can be partly transferred to the FFC on Ceres too; as such craters also show radial, linear and polygonal fracture patterns. Buczkowski et al. (2018) equally described moat structures next to the crater rim, almost the same manner as Class IV craters on the Moon.

The purpose of this paper is first of all a systematic description of the Class I craters of interest. Class IV Craters are excluded as they do not show clear-cut fissuring compared to Class I. In total we investigated thirteen FFCs with diameters varying from 26 km to 260 km and measured 2336 fractures. Predominantly, these craters are located in the mid latitudes between 60° S and 60° N. Fig. 1 illustrates a hillshade of Ceres' surface overlain by a HAMO-based digital terrain model (High Altitude Mapping Orbit with a resolution of about 135 m/px) (Preusker et al., 2016; Roatsch et al., 2017) that illustrates the global distribution of the thirteen investigated craters.

Cracks on Ceres' crater floors show a variety in morphological and deformational patterns themselves, on which we will concentrate in the following sections. The analyzation of the failure geometries and pattern will contribute to our knowledge of Ceres' surface conditions and its interior. Thus, the analyzation of fracture width, length, orientation and density can help to draw conclusions concerning the behavior of Ceres' surface material, physical parameters and the deviation of possible building mechanisms (Healy et al., 2017).

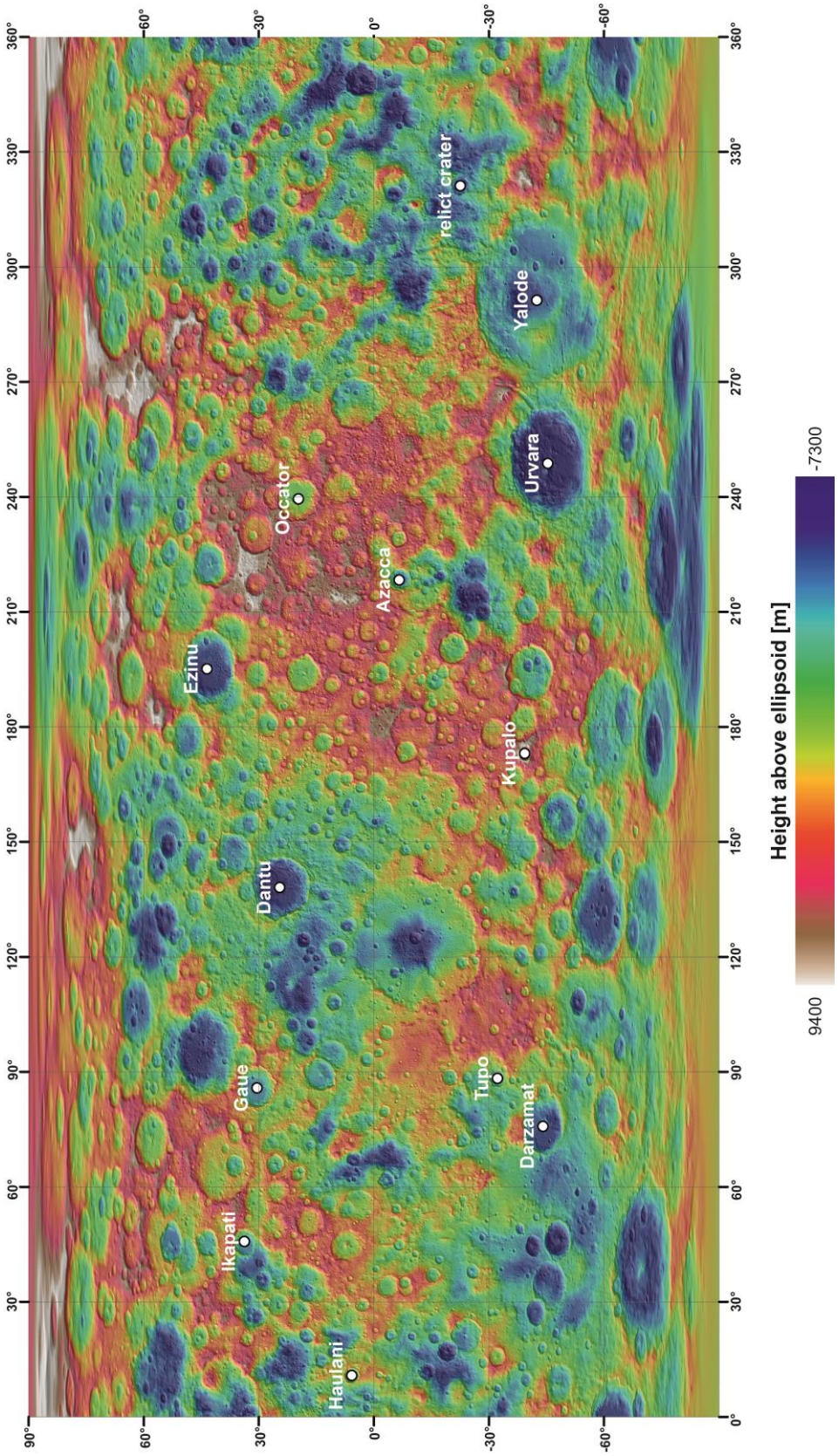

Fig. 1: Hillshade of Ceres (Roatsch et al., 2016) overlain by a HAMO-based digital terrain model (Preusker et al., 2016) (60% transparency) with the locations of the thirteen floor-fractured craters. The height difference (in white the highest and blue the lowest regions) is about 17 km. Note that there is no coherence between the height and the location of the FFC.

2 Data and Methodology

We analyzed the different cracks in the FFC concerning their length, width and orientation alike the distribution. All measurements were done for each individual crater fracture by determine the end points of its outcrop.

Length, width, and orientations are restricted to processes in coordinate geometry as data are only available in 2D and not 3D. The fracture map likewise only represents a size window. It can be considerably smaller than the scale range over which the linear feature is detectable (Singhal and Gupta, 1999).

In this study we use the FC clear filter mosaic of Ceres' Low Altitude Mapping Orbit (LAMO) with a resolution of about 35 m/pix (Roatsch et al., 2017). Additionally, a digital terrain model (DTM) derived by stereo photogrammetry is adducted for the compilation of profiles. This model is based on High Altitude Mapping Orbit (HAMO) images and exhibits a resolution of about 135 m/pixel (Preusker et al., 2016; Roatsch et al., 2016).

We use ArcMAP 10.3 for the analysis and mapping process to survey length, width, and orientation, and to generate cross-sections of the crater fractures to provide additional width information. Density maps are also an object of interest, as they help to visualize the distribution of the cracks.

The certain fracture length can be measured on any outcrop on the crater floors. For measurements in a uniform manner we had to determine a definition to reproduce the proceeding method. In our case the length is a continuous line, in some cases composed of two or more segments. It describes the distance the particular fracture can be traced, thus, the length between start- and end-point respectively. Fractures can be formed in any dimension especially by the interaction with smaller fractures. This makes it in some cases difficult to distinguish between individual fractures. In case of the mapping procedure it is important to notice that it is not feasible to trail the whole length of a fracture in the host rock. As described above the measured length only reflects the cut-off in a line segment that does not provide three-dimensional information (Rouleau and Gale, 1985). In this context there are three different biases that are also important to mention at this point: the censoring what means that ends, only one end, or none are apparent, the shifting of the data points and proportionate size as longer fractures preponderate (Priest and Hudson, 1981).

The fracture width is defined as surface trail. Fig. 2 reflects the location where the width is measured. The opening of the fracture is not constant along the whole fracture length. For that reason a number of width measurements were made for every single fracture. We measured a representative amount of width per fracture and build the mean value.

Because of the resolution, an accurate combination with cross-sections for adjustment is not reasonable in most cases.

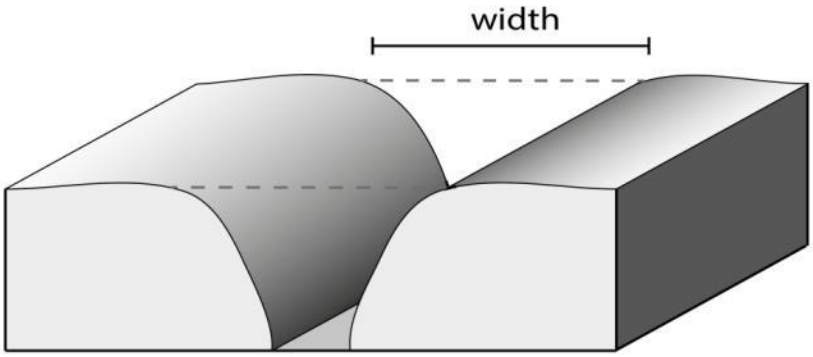

Fig. 2: Measured fracture-width according to the surface trail of the two crack sides.

The orientation of the failures is important to expose the tectonic history of the host rock and its behavior concerning,for example its strength (Healy et al., 2017). Rose histograms are the most common two-dimensional appliance to visualize such linear features, although they are susceptible to bias (Nemec, 1988). The circular histograms display the number of lineaments in compass direction. In this study each orientation is matched to one of ten degree classes (rays). The length of the rays corresponds to the percentage as a function of total measurements relating to the measured directions. The orientations were calculated by reading the geometry of the line data. Afterwards the influence of the lines can be weighted by multiplication of the length respective. That reduces the influence of the fracture so that short lines will take less account than longer ones. This is especially useful if one fracture is segmented into many smaller ones, like some crater fractures in our study case. Otherwise these fractures would be considered as many small cracks trending into the same direction what would lead to an excessive or rather artificial “strength” in the particular class.

Based on our observations, we also generated a fracture density map to visualize the distribution of fractures in the craters described above (Fig. 10). This is necessary as the patterns, shapes and physical parameters of the crevices can deliver important information to constrain and draw conclusions concerning the floor-fracture formation processes, for example the physics of these processes, the behavior of the surface material and/or insights of the target (Healy et al., 2017; Sato et al., 2010). Thus, fracture density maps are also suitable to provide information concerning shear fracturing by interaction of constituent fractures (Moore and Lockner, 1995). Therefore, the fracture density ensures to accentuate those regions, that imply high dense fractures and helps to make predictions concerning the extension of fracturing.

Based on this, the magnitude-per-unit area in square km has been calculated from the measured line features that fall within a certain radius around each cell. These were provided by the special analyst tool *“Line Density”* in ArcMAP. Impact crater that contain a high population of floor fractures or networks within a high interconnectivity like in Dantu or Occator crater, will form regions with higher

fracture density than those with less terse spaced ones (Rodríguez et al., 2005).

3 Characteristics of floor fractures on Ceres

Typical FFC on Ceres contain an irregular shaped rim, mostly deformed by slumping or sliding of the crater rim building wall terraces, and/or a central pit or peak. While in several FFC some regions of the crater rims are largely "destroyed" by slumping of the wall, the opposite flank of the rim appears to be fresh and steep. Fractures on the crater floors are in general of concentric, radial or polygonal shape. Those are most consistent with the Class I lunar FFC. Floor-fractured craters with a moat structure on the other hand share similarities with Class IV lunar floor-fractured craters (Buczkowski et al., 2018). Because of the morphological differences compared to Ceres' FFC we will not refer to the remaining classes.

The fracture morphology in most cases is characterized by an irregular pattern with concentric and/or radial shape. They are located on the floor and in some cases on the ejecta blanket of the crater circumferential to the crater rim (Fig. 4). Some fractures originate from slumping of the crater rim and build tear-off edges. In a few cases, this extended rim failure produces peripheral concentric graben.

Other fractures are approximately straight and subparallel to parallel (Fig. 3d). Occasionally, those with slight sinuosity character are also noted. Frequently observed are crevices that merge into various branches or narrow fissures that conjoint into straight wide fractures. There, the failures bifurcate into grand fracture groups or networks that can cover up nearly half of the crater floor. Dantu and Occator crater are some of the examples of such pattern (cf. Fig. 3 b and c and Fig. 4b and i). Another peculiarity is the transition of "normal fractures" to pitted lineaments or narrow discontinuous crevices obvious especially inside Dantu crater (Fig. 3 b). Occasionally, these pit chains are recognized on the extension or terminus of the lineament. Usually they connect crevices at the opposite end, except in Ikapati crater (see Fig. 3 a).

In case of Occator, the surface between fractures and the environment of the fractures contains blocky fragments in some regions that seem to limit the tear hiking (Fig. 3c). Others are cut by slides. Because of their locational and chronological diversity they point out a complex formation scenario in Occator crater.

Another interesting fracture type is located in Yalode crater. Its fractures are wider and more developed than in other craters. At least two different generations can be described, therefore , they should yield the terminus fault. However, fractures show high variations in shape, width and length inside one crater. They also contain deformational features such as en échelon structures and possible strike slip faults, dilatational jogs or tilted blocks.

Because of the variations in morphology it is likely that the fractures and floor-fractured craters

themselves do not share one single formation history.

Fig. 4 depicts clear filter images of the thirteen craters with its mapped cavities while Table 1 and Table 2 include the different attributes of those.

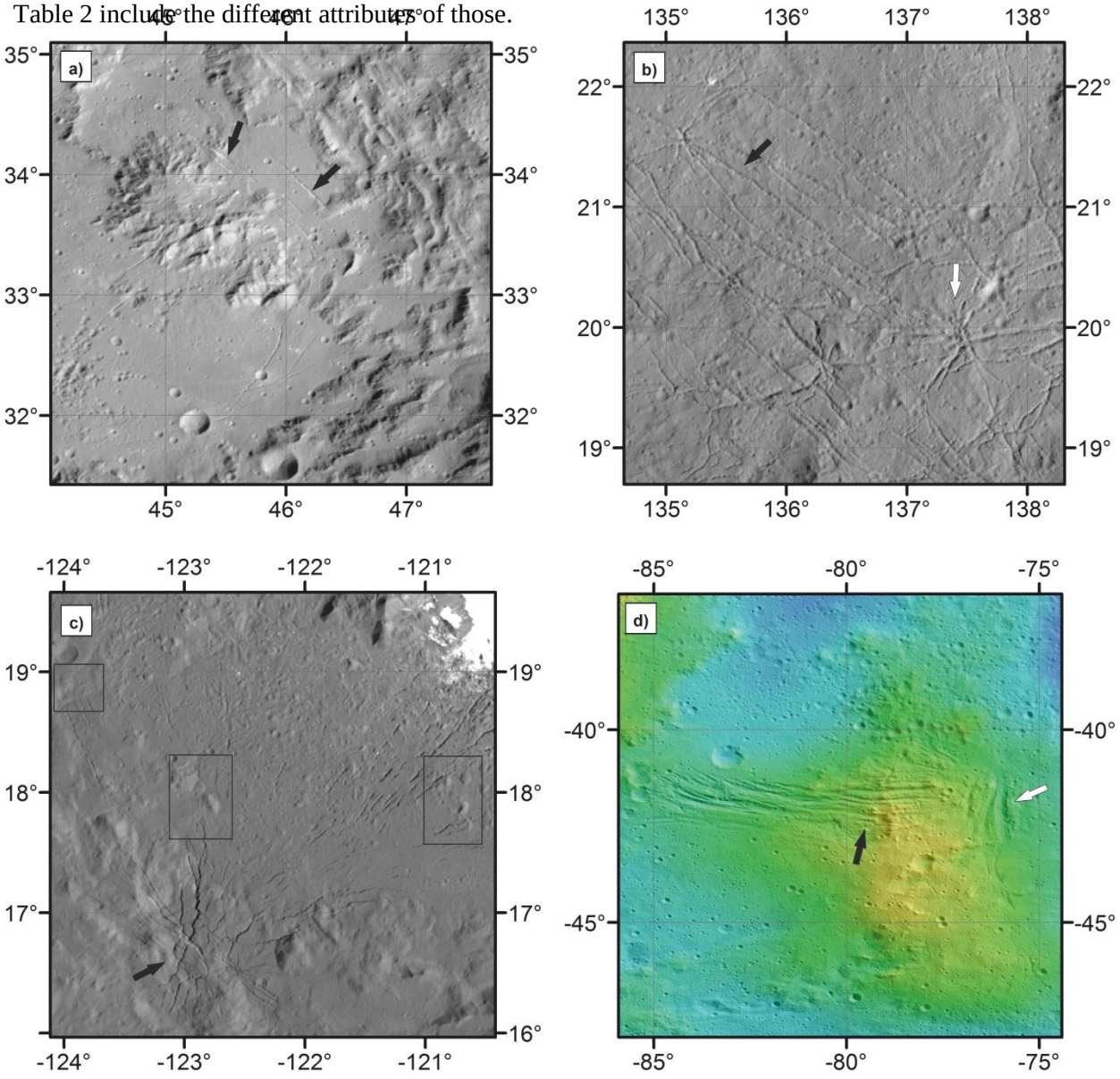

Fig. 3: Zoom onto a selection of crater floors. a) Floor fractures in Ikapati crater. Note the pitted fractures that border the central ridge structure (black arrows). They are oriented parallel to the huge rim slumps. b) Network of fractures in Dantu crater with pit ends that tie the lineaments (black arrow). The white arrow demonstrates the spider like fracture pattern possibly originated by sources from the subsurface. c) Cracks on the floor of Occator crater that also form a network. In contrast to Dantu crater, the fracture pattern is more local and composed out of radial and concentric fractures. The black arrow demonstrates a possible upward force under the surface. The black rectangles encircle examples of blocky surface components that limit tear hiking. d) Clear filter image of Yalode crater overlain by a HAMO DTM. Note the at least two generations of parallel cracks (black and white arrow) in a T shape arrangement possibly with a dependency of the height. The Yellow color corresponds to high terrain while the lower ones are blue.

Crater	Azacca	Dantu	Darzamat	Ezinu	Gaue	Haulani
Location	6.6° S; 218.4° E	24.3° N; 138.2° E	44.2° S; 76.4° E	43.2° N; 195.7° E	30.8° N; 86.2° E	5.8° N; 10.8° E
Diameter [km]	50	126	92	116	80	34
Morphological specifics	Flat crater floor Landslides and hummocky terrain at northern half of the rim Steep crater walls	Flat crater floor Landslides and hummocky terrain at the rim Destroyed NE-part Steep crater walls	Flat and old crater floor Relict landslides Partial steep flanks	Flat and old crater floor Ancient landslides	Flat crater floor Steep flanks on the NW rim Landslides on the SE rim	Smooth flat crater floor Pits Landslides Steep flanks
Fracture pattern	Radial fractures at the center next to the central ridge	Radial and concentric Concentration on the south-western half of the crater Few fractures next to the central ridge Fracture build grand networks Transition to pitted lineaments	Possible concentric fracture at the northeastern flank of the crater	Fractures build central graben Wide radial fractures	Short fractures circumference the central pit some radiate linear to the rim	Concentric fractures on top of smooth slides
Possible fracture deformation	Step over Shearing	Shearing	—	—	—	—
Fracture on the ejecta	X	—	—	—	—	X
Peak/Pit	Central ridge	Central ridge	—	Central graben	Central pit	Central ridge

Table 1. Characteristics of the thirteen floor-fractured craters on Ceres.

Crater	Ikapati	Kupalo	Occator	Relict crater	Tupo	Urvara	Yalode
Location	33.8° N; 45.6° E	39.4° S; 173.2° E	19.8° N; 239.3° E	22.5° S; 321.2° E	32.3° S; 88.4° E	45.6° S; 249.2° E	42.5° S; 292.5° E
Diameter [km]	50	26	92	38	36	170	260
Morphological specifics	Asymmetric formed Landslides between N an S Flat and smooth crater floor on the SW flank	Flat crater and smooth floor Landslides Steep flanks	Flat crater floor Landslides and hummocky terrain Flows	Old crater floor	Hummocky crater floor and landslides One big soil	Flat crater floor Hummocky terrain and landslides especially on the southern rim	Flat crater floor Landslides and hummocky terrain
Fracture pattern	Parallel and radial to the centraldome Pitted lineaments Small fractures concentric to the rim on top of slides	Concentric to the crater rim on top of slides	Radial and concentric Fractures start network on top of landslides Surround the central dome Get cut by morphological diverse regions	Concentric fractures on the NE crater rim	Concentric fractures on the crater rim and slides	Radial fractures Concentric fractures on the crater rim	Radial fractures Concentric on the crater rim Very wide linear fractures in the western part of the crater
Possible fracture deformation	__	__	__	__	En èchelon	En èchelon	horst/graben or book shelf
Fracture on the ejecta	X	(X)	X	(X)	__	(X)	__
Peak/Pit	Possible ancient central dome	Central ridge	Central dome	__	Central ridge	Ancient central ridge	Ancient double ring?

Table 2. Characteristics of the thirteen floor-fractured craters on Ceres.

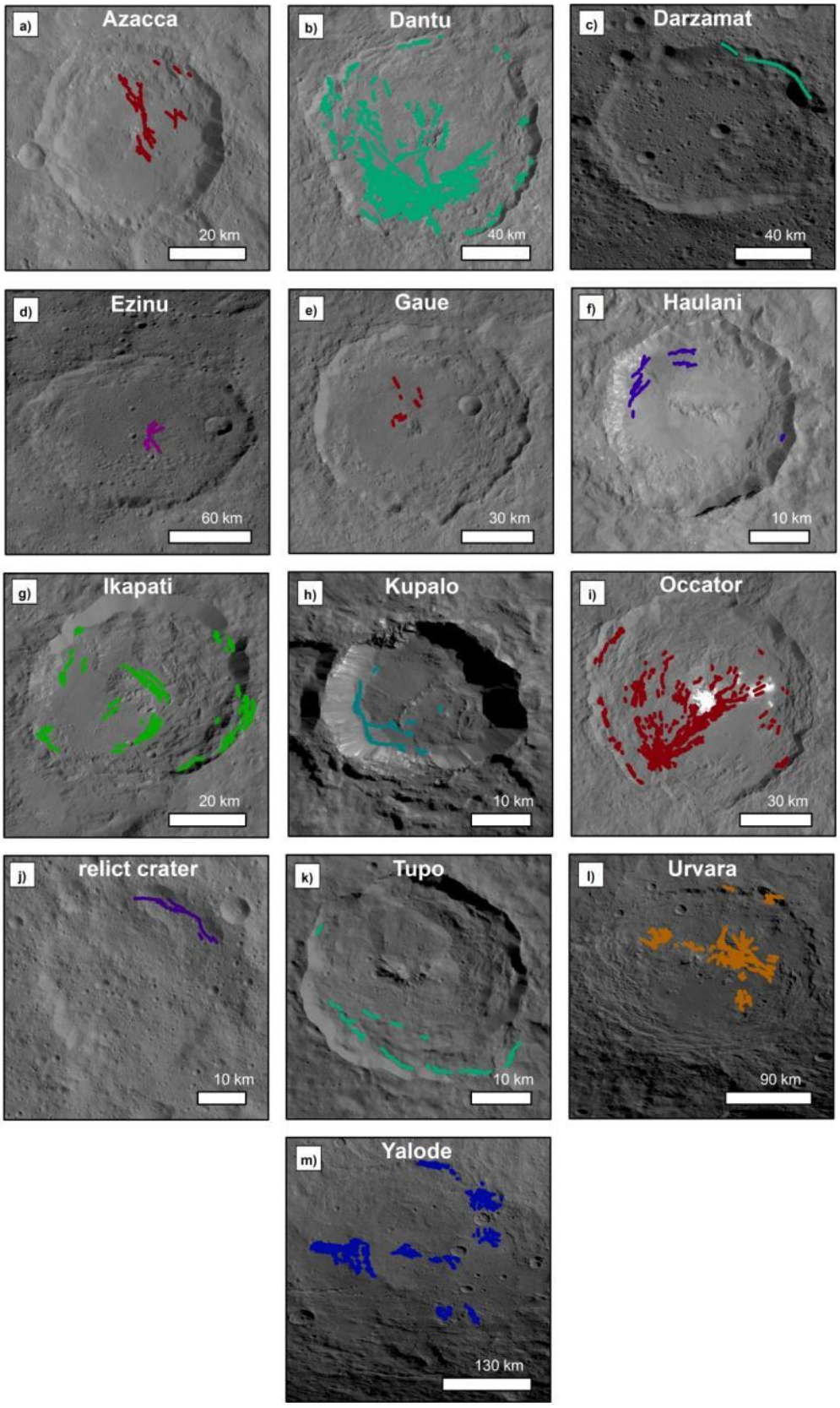

Fig. 4:. Clear filter images of the thirteen floor-fractured craters on Ceres with mapped fractures on the crater floors. We observed radial a), d), e), m) and concentric fracturing in c), f), g), h), j), k). Some craters show both types of fracturing or grand networks like in b), i), l) or m). Note that some craters show circumferential fractures, too, like Haulani, Ikapati, Dantu, Occator or Azacca crater.

3.1 Measurements of floor fractures

Trace-length of fractures

The fracture length has been measured on the outcrop of every single fracture. Fig. 5 illustrates a selection of histograms of the frequency plotted against the trace-length. The uppermost image comprises the entire amount of fracture length, while the lower ones represent the frequency of fractures for a selection of four craters. The maximum length of all cracks is about 41 km. Nevertheless, it is obvious that most of the failures are relatively short as the average length in total varies between one and three kilometer. Every histogram shows a decreasing number of fissures by increasing length. Especially in case of Dantu and Occator crater this is conspicuous and can be explained by the integration of those numerous small fractures that build complexes or merge to larger ones. Faults in Yalode on the other hand show wide and large generations that are located subparallel to parallel. This also is mirrored in the wider range of fracture length in Fig. 5. Nevertheless, a decrease in the crack length is also evident in this case.

As described in chapter two, the length only represents a cut-off in a two-dimensional system. Therefore, the real distribution of the fracture length in Fig. 5 histograms has to be shifted to the right side.

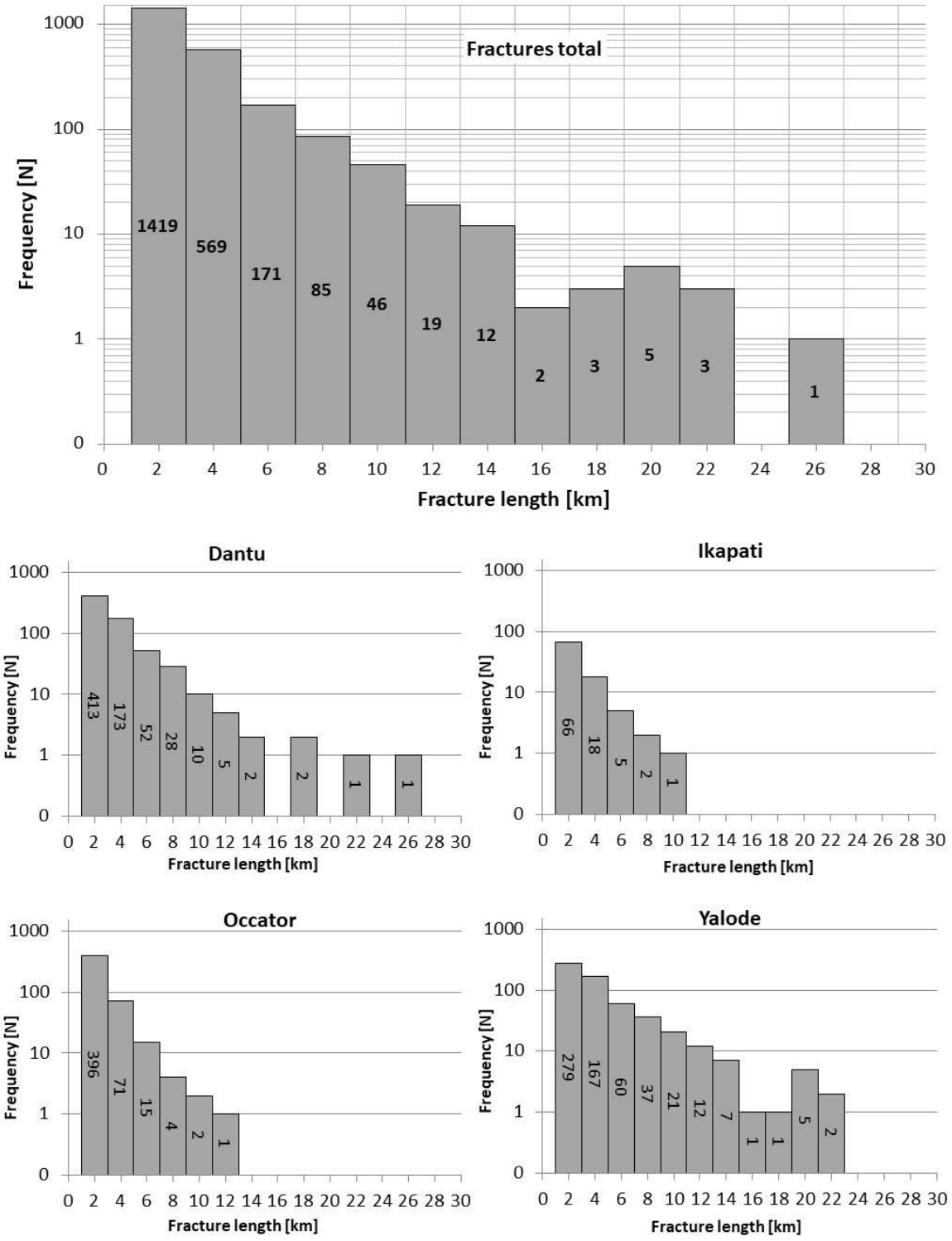

Fig. 5: Histogram of the frequency of fracture length. In the uppermost histogram the frequency of the total amount of fractures is shown. The histograms show exemplarily the distribution for four craters.

Width of fractures

The width of the fractures is also measured for each floor-fractured crater. In case of Ceres, not every fracture shows a uniform habitus and varies within the particular crevice. Most of them are relatively small and narrow, except in Yalode crater. There, for instance, fractures appear to be graben- like and/or tilted book-shelf structures.

Fig. 6 comprises the histograms of the frequency plotted against the fracture's width. The uppermost histogram includes the total amount of fracture width. The remaining histograms were made equivalent and show the same selection of craters as in Fig. 5. Fractures on Ceres do not show a high variance in width and are all relatively narrow. In total the maximum width varies from several meters up to a few kilometers with the highest amount in the 200 m and 300 m range and a total average of about 231 m. Only Yalode and Ezinu crater show some deviation. Yalode crater depicts frequencies with increasing width up to 2 km and Ezinu with its central graben in a similar magnitude.

We plotted the width against the length to determine if there is a relation between the both instances length and width (Fig. 7). However, the high dispersion describes that apparently there is no clear relation between the length and width.

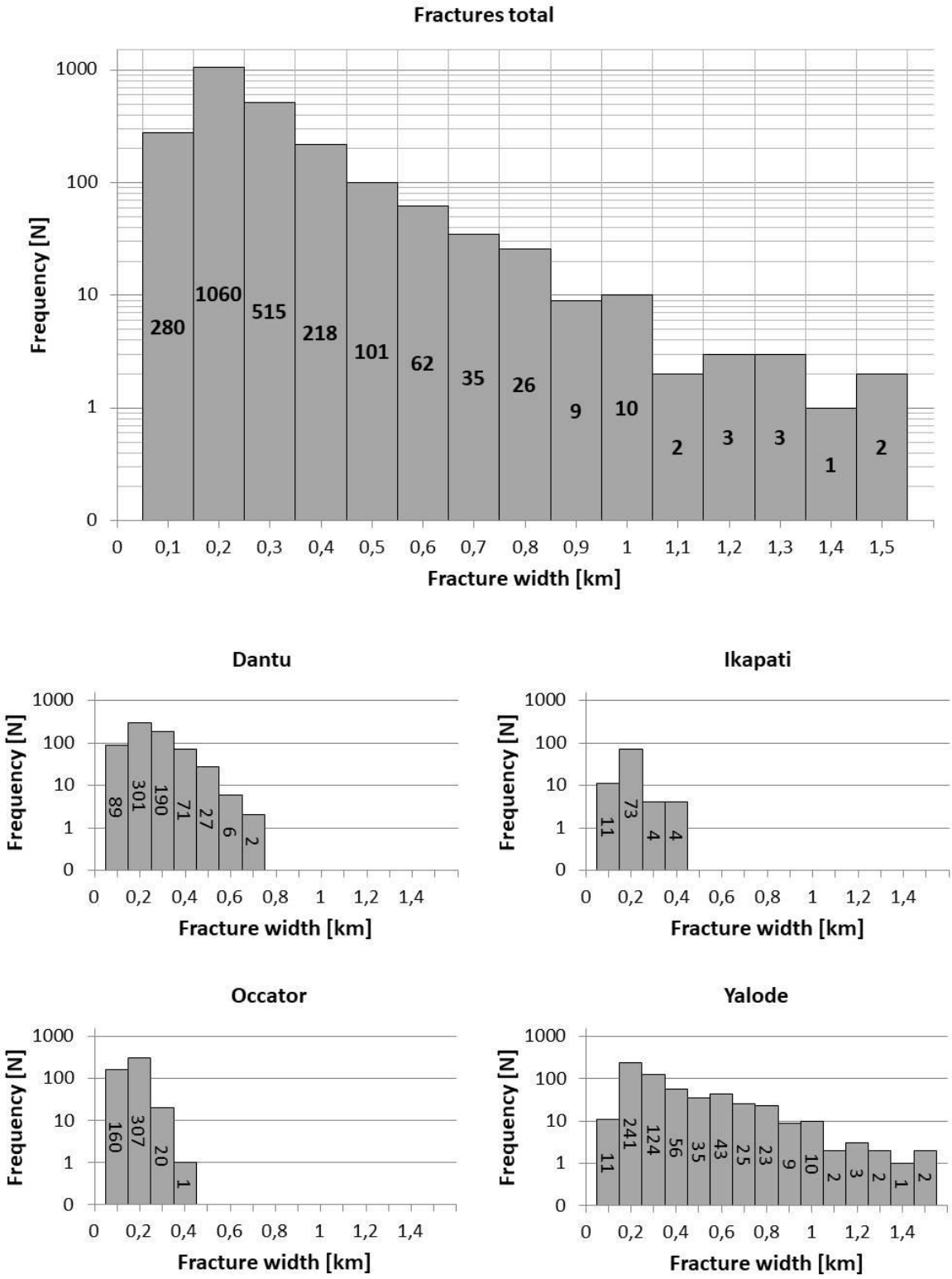

Fig. 6: Histogram of the frequency of fracture width. The first one shows the frequency of the total amount of fractures. The following show the distribution for the particular craters.

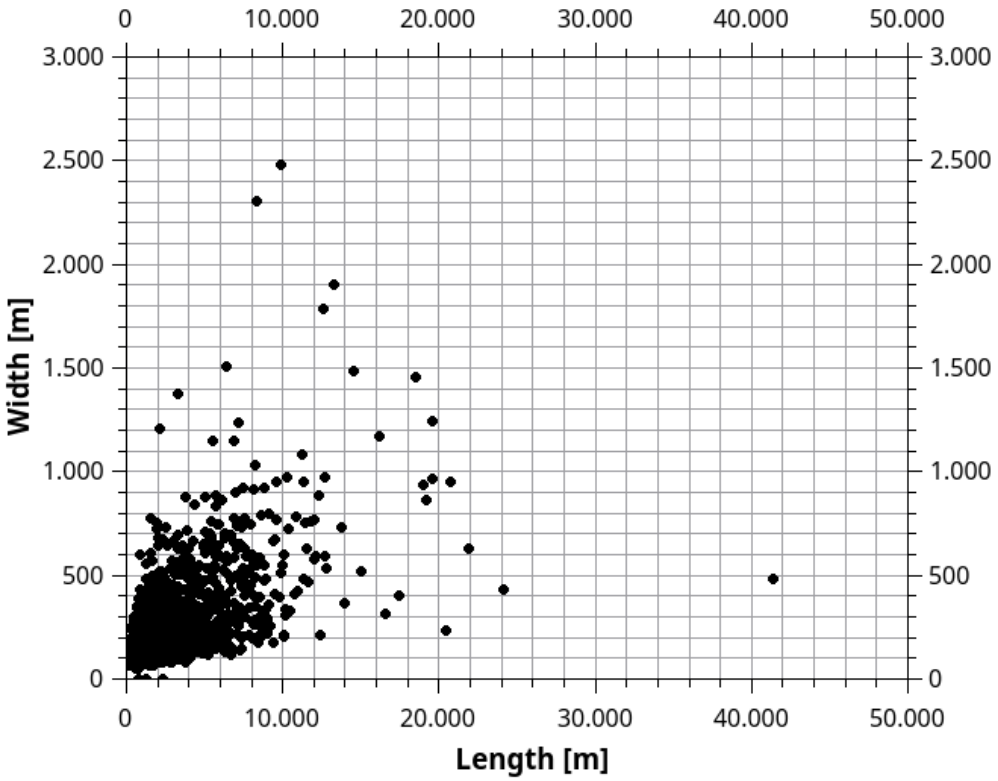

Fig. 7: Histogram of width versus length showing no clear relation between length and width discernible on the basis of the high dispersal of data points.

Fracture orientation

Fig. 8 displays the different rose histograms of the thirteen research craters. Discernable by the basis of distribution of rose histogram rays, almost every crater exhibits fractures trending in two or more different directions. They point out the different fracture types such as concentric and/or radial pattern. Although the orientations for each particular crater are consistent in itself, globally they differ from each other with no indicated trend as expected. This reveals that they are globally independent and share no single formation event. We also plotted the frequency against the striking to test this hypothesis, and found out that there is a bimodal distribution with a two maxima offset by almost 90° azimuth. Furthermore,there is only a slight maximum in the 130° and 150° region tops (cf. Fig. 9), therefore, this assumption can be excluded.

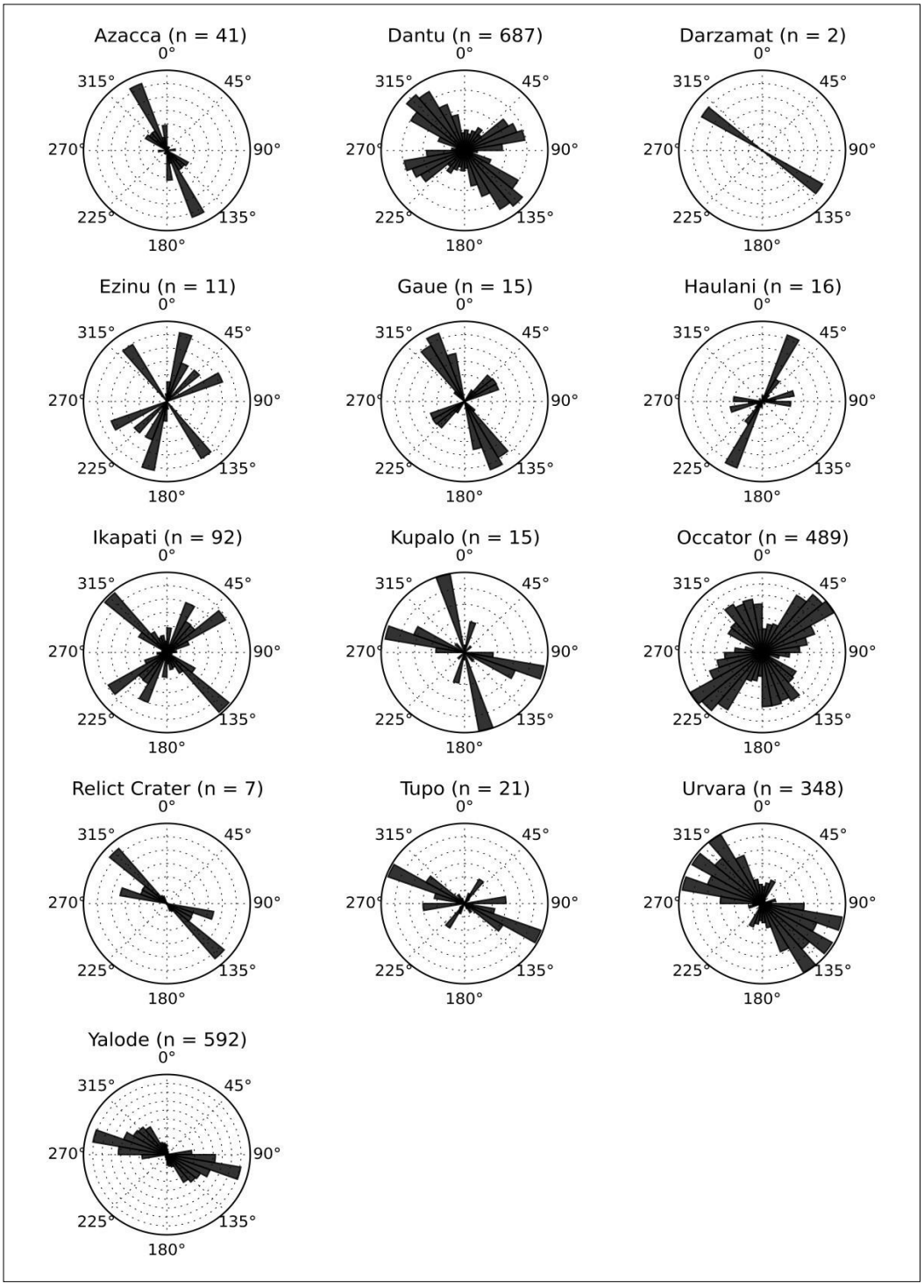

Fig.: 8: Rose histograms of the different FFC weighted by the fracture length. a) Azacca crater with a NW-SE preferred orientation, b) Dantu crater shows three preferred orientations in NW-SE, E-SWW and a small value in NE-SW direction c) Darzamat only contains few fractures and is therefore not representative d) Ezinu contains chaotic orientations mostly between NE-SW direction e) Gaue contains two dominant preferred orientations in SE-NW and NE-SW direction f) Haulani's fractures show a preferred directions to NE-SW g) Ikapati crater illustrates a wide distribution h) Kupalo contains fracture orientations that are concentrated between the SE and NW region i) Occator also contains at least two main orientations. These concentrate in the NE-SW and SE- NW direction j) the relict crater also has only a few fractures that are not representative with a slight rise in SE-NW direction k-m) Tupo, Urvara and Yalode crater show a great amount of fractures orientation between SE-NW with no significant deviations.

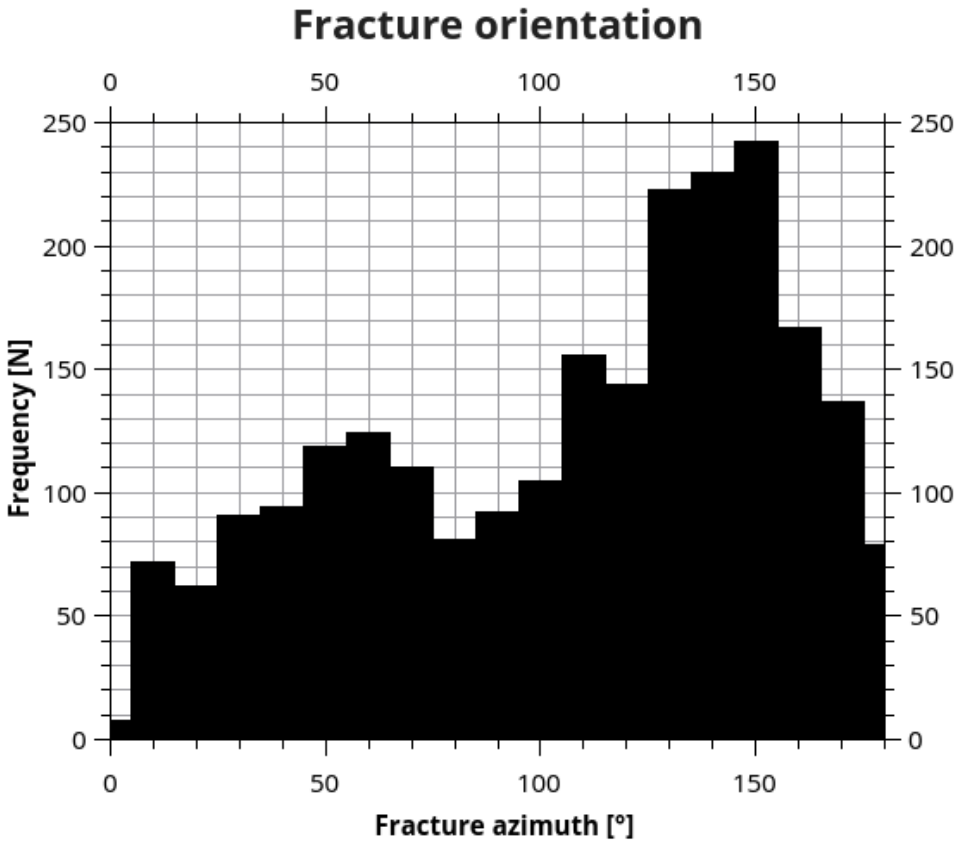

Fig. 9: Histogram of fracture orientations plotted against the frequency in percentage. The distribution of the striking directions shows a slight tendency in the 130 to 160 degree region.
Nevertheless, the difference is too small to speak of a definite global preferred orientation.

Fracture density

Elder et al. (2012) suggested that in case of impact induced fracturing the fracture density should decrease with increasing distance from the crater center. They also described that the material beneath an impact crater will be also fractured. However the largest volume of void space would be located beneath the center of the crater (Elder et al., 2012).

Fig. 10 illustrates the density map created from the distribution of floor-fractures on Ceres. In violet are the regions with a high fracture density and in turquoise are those with a low density. Compared to the assumptions of Elder et al. (2012) our density map shows a slight antithetic observation. While a lot of crater fractures are located next to the crater center just as many are concentrated on the crater rims, especially in larger craters with higher fracture density. Specifically in Dantu and Occator crater as well as in Yalode and Urvara crater a concentration of the fractures to the rim is more common.

Another point is that the material beneath the floor-fractured craters is not necessarily fractured.

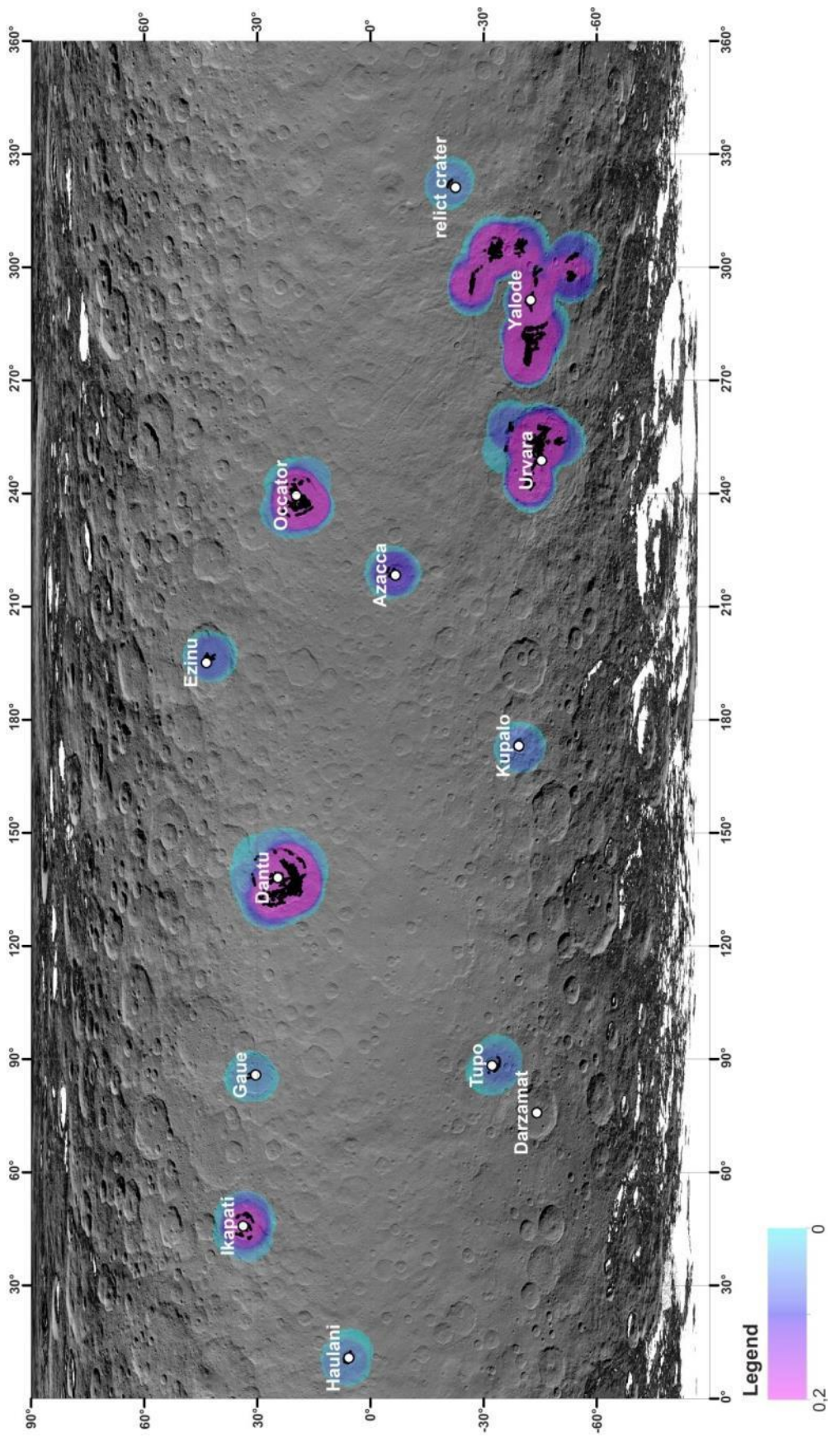

Fig. 10: Lineament density map of the thirteen FFC on Ceres. Note the distribution of fractures is concentrated in the center and on the crater rim of the craters, with a high density in violet and low density in blue color. The mapped fractures are the line features in black.

4 Discussion

Our key observations can be used to interpret and constrain possible material properties of Ceres' surface, to derivate physical assumptions, and to discuss formation mechanisms in conjunction to the relative time flow of crater processes. The present study provides a framework concerning the crack's morphology, physical parameters such as length, width and orientation as well as a density map. Problems concerning the mapping and measurements are related to low resolution of the DTM and mosaic, and changes in brightness and illumination. Therefore, the accuracy or precision of our study is limited. An error for mapping single structures is estimated to be several tens of meters.

Additional sources of errors are the mapping scale and the manual mapping process itself. At this point some fractures were probably missed out.

On Ceres there is only a small amount of floor-fractured craters. We found out that the distribution and population of these craters and their fractures varies spatially, lithology, and structurally throughout the study area. The main descriptive statistics deduced from the length, width, orientation, and density measurements of fractures show that cracks on Ceres are share no uniform senses of direction syndetic on the craters. Hence, preferred orientations are only visible for each crater itself. Width measurements point out, that fractures are relatively narrow. There is no correlation between length and width. Only in some cases, for example in Yalode crater, fractures are wide and more distinct and illustrate a possible connectivity to crater internal height differences in combination with rotational blocks (Fig. 3d). Hence, in this case a tectonic process in the underground is reasonable.

4.1 Material dependency that facilitate fracturing

Some material compositions and properties on Ceres' surface facilitate the mechanism of fracturing as well. The material compositions of the target function as a factor in determining the deformation properties of the rock (Nelson, 2015). Low temperatures and low pressures for example lead to the alteration of the material bonds. At high strain rates, for instance, atoms behave more static so that the material tends to fracture. Materials in the low temperature regions, the so called permafrost rocks, on the other band possess a reduced shear resistance. This also favors the process of fracturing for example along rock-ice boundaries for low normal stresses (Günzel, 2008; Krautblatter et al., 2013).

Based on studies, the surface of Ceres is made up of a differentiated rock or rock-ice mixture, mentioned in section one. The main components are phyllosilicates (ammoniated, Mg-, Na- bearing), carbonates and dark material with some parts of H_2O-ice (Ammannito et al., 2016; Castillo-Rogez and

McCord, 2010; Combe et al., 2016; De Sanctis et al., 2015; Park et al., 2016). Carbonates for instance are of brittle nature and susceptible to fracture (Moore, 1989; Nelson, 2015). Although the phyllosilicates or clay-like minerals behave in a more ductile manner, we suggest that the heat induced by the impact process could lead to the alteration of the surface material and, therefore, a change in the material properties to the point of brittle fracturing. In contrast, the H_2O-ice bearing parts should act in a similar manner as permafrost rocks, which involve a combination of reduced shear resistances that leads to fracturing as well . Hiesinger et al. (2016) also assert that Ceres' crust should be heterogenic deviated from the transition of simple to complex craters. The outer shell composed of a rock-ice- mixture would allow a limited relaxation of the craters. Thus, we confirm as the surface of Ceres has to contain at least brittle components that favor the mechanisms of fracturing. Scully et al. (2016) also described linear features on Ceres as an indicator for a strong outer layer not dominated by viscous relaxation. Samhain Catenae a grand linear feature located in the environment of Yalode crater, would argue for an origin by uplift and extension induced by an upwelling region coherent to predicting models (Scully et al., 2016). This aspect could also explain the formation of floor-fractures and would favor the widening of fractures especially in case of Yalode and Urvara crater in the proximity.

4.2 Physical mechanism that describe fracturing on Ceres

In general, the origin of fractures is based on stresses produced by different mechanisms, such as: (a) tectonic stresses related to the deformation of rocks; (b) contraction due to shrinkage by cooling melting or desiccation of material; (c) remaining stresses due to pre fracturing events; (d) surface movements such as landslides; and other. Extensional fractures comparable to those in Yalode crater would be caused by the dilation of these cracks e.g., by dissolution (Singhal and Gupta, 1999). Usually, the process of cracking and rupture of rocks is related to shock-induced damaged material of the target, followed by the collapse of transient cavities that decreasing away from the rim zone (Salguero-Hernández et al., 2010). Elder et al. (2012) likewise suggested impact induced evolution of floor fractures. These should be located near the crater center and also align the environment of the rim. Our density map Fig. 10 illustrates as a function of the quantity of fractures that floor-fractures are not only concentrated next to the crater center. A decrease to the crater rim is also unneglectable as in some cases there are no fractures on the ejecta or the environment of the crater rim at all. Therefore, the main building mechanism of floor-fractured craters in case of Ceres is not solely impact induced by the compressive shock wave, the release of the refraction wave, and by shear deformation during the expansion of the cavity as Collins et al. (2004) and Elder et al. (2012) described as common formation mechanism. Rather some fracture patterns describe processes related to tectonics or the loss of volatiles.

As described above, Ceres' floor-fractures also reveal some deformational features in the regime of tension and/or contraction, for example the release of pent-up stresses in the material driven by mechanisms such as tectonic extensional forces, cooling, and/or desiccation by the loss of volatiles. Here we discuss the following likely formation mechanisms:

- En echelon: Structures within rock caused by non-coaxial shear (Fig. 11).
- Horst and graben structure: Horst and graben are regions that lie between normal faults and are either higher (horst) or lower (graben) than the area adjacent to the faults (Fig. 12a,b).
- Shearing: Lateral movement of one rock surface against another (Fig. 11).
- Tilted blocks: rotational extension on planar faults, which results in a uniform rotation of faults and crust (Fig. 12 c,d).

Fractures interpreted as en échelon structures, for example, demonstrate the shearing of the failure to sigmoidal pattern. The direction illustrates the sense of shearing (Durney, 1973; Pollard et al., 1982). Those, fractures are formed before the material loses its complete cohesion (Engelder, 1987) and are distinct in craters like Tupo or Urvara crater. In case of Tupo this structure possibly is developed by shearing induced by an impact next the crater rim (Fig. 11). Parallel fractures, for example in Yalode crater, impart a strong anisotropy to the target material. We interpret these features as possible horst and graben or half graben systems. Apparently, they are in the v-shaped angle of incidence. They reflect the brittle manner of extension of the host rock comparable to graben on the Moon or horst and graben structures on Ganymede. Fig. 12 shows a pictorial representation of such mechanisms. Uplift and extension induced by an upwelling region assumed for Samhain Catenae would also argue for the widening of these fractures and reflect a tectonic induced origin (Scully et al., 2016). On the other hand, a greater number of more interconnected fractures like in Dantu or Occator crater tend to reduce the anisotropy of the rock (Singhal and Gupta, 1999). For instance, the largest amount of small fissures in Occator and Dantu crater could denote that in case of fracturing the energy tends to divide on many smaller fractures to avoid one single crack. Chasm that are pre-existing in the target material would enable such mechanism (Krönert and Böhm, 1980). As described in the previous sections, fractures on Dantu's floor build up grand networks with lineaments that extend in pit ends or pit ends that tie two or more lineaments. In general, pit ends can give specific information on the formation of fractures in the FFC. Associated mechanisms for pits are (a) the collapse of chambers or tubes; (b) lose material that attain pre-existing fissures beneath the surface; (c) dike intrusion; (d) dissolved material (also ice); (e) extension fractures (Wyrick et al., 2004). Mars and Vesta are examples where pits are interpreted to be formed by the impact process that releases volatiles by degassing (Boyce et al., 2012; Denevi et al., 2012). Pits on Ceres are also supposed to be related to a rapid outgassing of volatile-rich material such as hydrated salts or ground ice especially in case of Haulani and Ikapati (Russell et al., 2016; Sizemore et al., 2017). Thus, we

suggest that in case of Ceres' FFC the mechanism of degassing or resolving of volatiles is also involved in the process of fracturing.

Fractures that radiate from one single location like in Occator crater reflect fracture structures typical for surfaces that get affected by sources from beneath the underground, such as up-doming of material or an intrusion of low density material from below. Ahuna Monshas been interpreted as a cryovolcanic extrusive dome on Ceres (Ruesch et al., 2016; Russell et al., 2016) concludes the possibility of cryomagmatic intrusions for the formation of Ceres FFC (Buczkowski et al., 2018; von der Gathen et al., 2016).

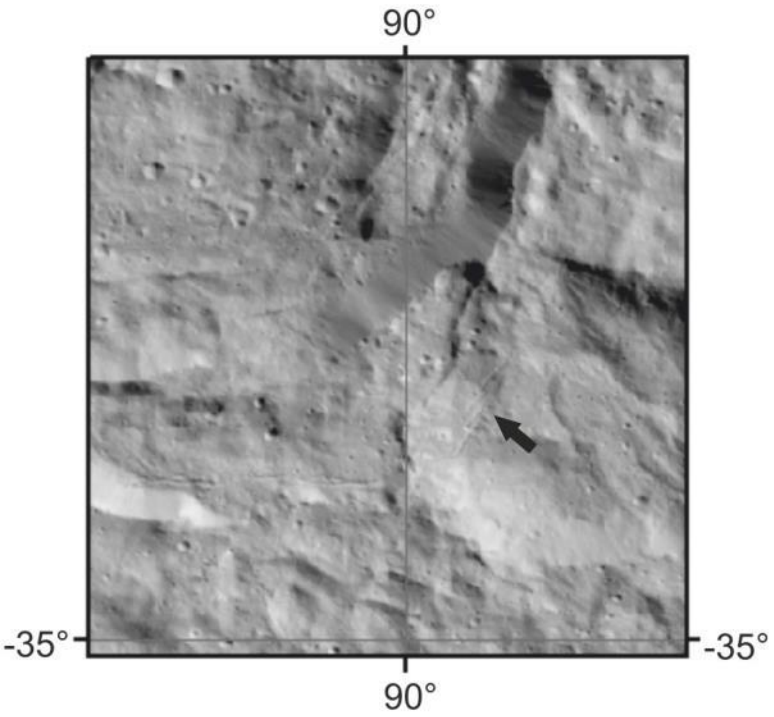

Fig. 11: South-western rim of Tupo crater that shows en échelon structures on its rim (black arrow) probably controlled by the small crater in the eastern part of the image.

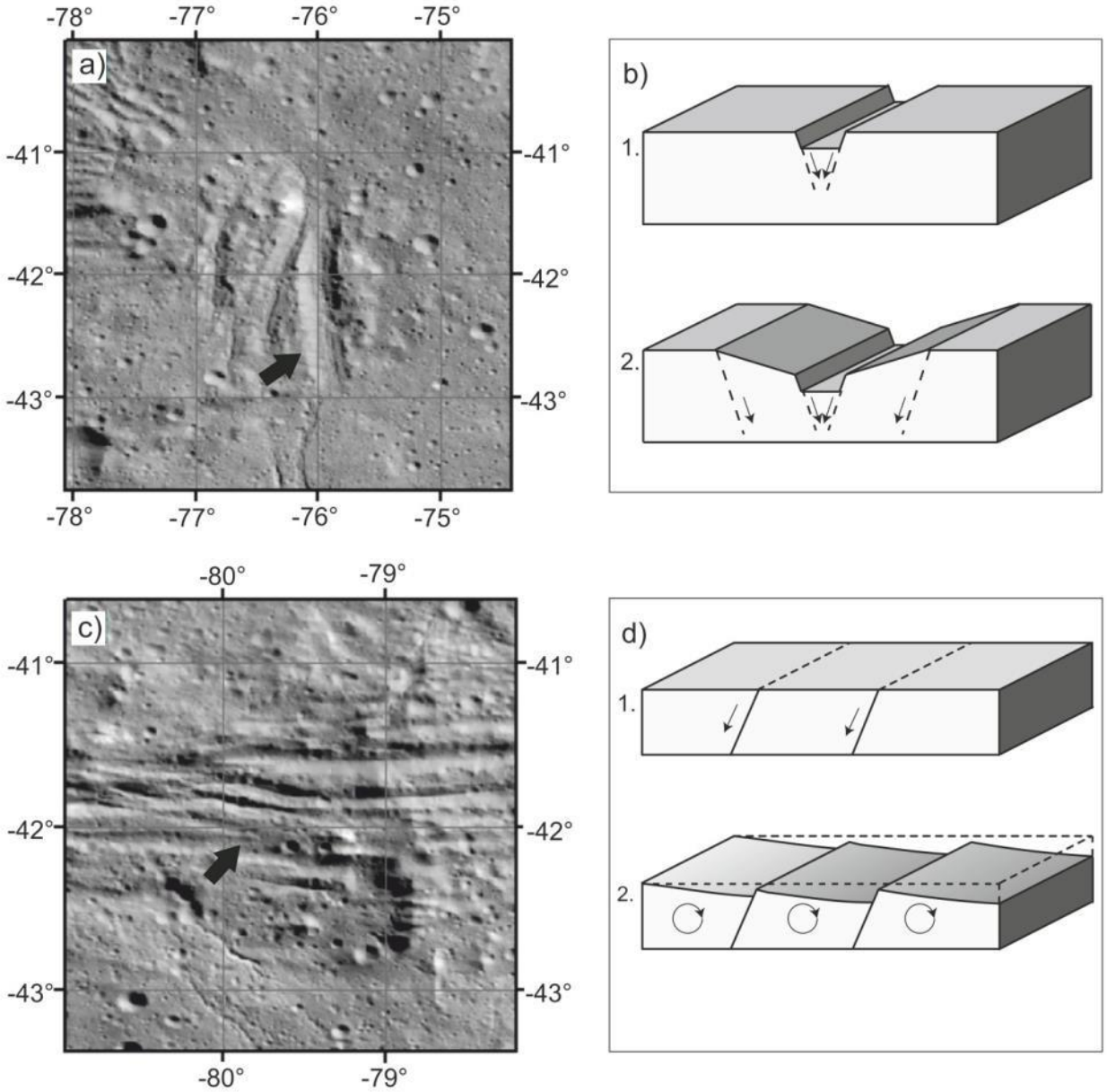

Fig. 12: Linear fractures in Yalode crater. a) possible horst and graben structures on the clear filter image whilst b) theoretical formation mechanism of the small and graben structure. c) possible tilted block structures with the coherent theoretical model in d).

4.3 Formation mechanisms of FFC in the solar system

Floor-fractured craters have been observed on different planetary bodies in the solar system like Moon, Mars, Venus, Mercury and icy satellites (e.g., Korteniemi et al., 2006; Schultz and Orphal, 1978; Wichman and Schultz, 1995b). FFC on the Moon were first described by Schultz (1976). He published a classification scheme and specifies particular criteria of the morphologies of these craters. The scheme includes the characteristics concerning the crater floor, wall, and rim zones and builds the basis to derivate six different classes (Schultz, 1976). He precises' floor-fractured craters as ones that contain radial, concentric, or polygonal fractures within the crater floor. A number of craters also show modification features including graben-like moat structures, coherent floor uplifts, and various degrees of central volcanism interpreted as a coherently uplifted central floor plate (Jozwiak et al., 2012; Schultz, 1976). The crater depth decreases with greater degrees of floor deformation and the majority of failure becomes concentrated near the floor edge. Central peak reliefs are typically unaffected by this uplift. Another conspicuity is that such floor-fractured craters are much shallower than primordial craters of similar size (Schultz, 1976). In the literature, various theories concerning the origin of the Moons' floor-fractured craters are discussed. Typical building mechanisms are the extension beyond the crater rim and appear to be unrelated to more regional fracturing in the environment of the crater. Another explanation for FFC is topographic relaxation and magmatism beyond the crater center. Such so called viscous relaxation would give a reasonable explanation for the observed broad crater floor uplifts, with limitations in explaining some of the modifications (Hall et al., 1981). On the other hand, a model of Dombard and Gillis (2001) predicted that viscous relaxation of crater floors is unlikely to cause fractures on crater floors with diameters < 60km on the Moon. More explanations include the deformation of craters over shallow crater- centers by igneous intrusions that would cause local uplift. But this theory seems not as susceptible (Hall et al., 1981; Schultz, 1976; Wichman and Schultz, 1995a). It is difficult to distinguish between formation models of lunar floor-fractured craters as crater floors can comprise both: uplift induced by magmatic intrusions beneath the crater (Jozwiak et al., 2015; Jozwiak et al., 2012; Schultz, 1976) and shallowing by viscous relaxation (Hall et al., 1981).

Some craters on Mars exhibit similar floor-fractured craters as those on the Moon (Schultz, 1978; Schultz and Orphal, 1978). Their characteristics are for example floor fractures, uplifted floor plates, moats, proximate lava plains, and filling lava flows. These features point out an intrusive and eruptive volcanism controlled by the crater (Schultz and Orphal, 1978). Although there are some differences in the morphologies of FFC on Mars and Moon, the lunar classification scheme has been partly adapted for floor-fractured craters on Mars. One difference is,for example that moats are more extensive and a wider system of fractures, interpreted as volatile-induced enhancement of the fracture formation (Schultz and Orphal, 1978). Polygonal fracture systems are also more common on Mars and indicate repeated periods of floor uplift and subsidence (Korteniemi et al., 2006). Another difference between

FFC on the Moon and Mars are their formation mechanisms. Schultz (1978) for example, described that these crater morphologies can be formed by the closure of former depressions. This would suggest that once a water/ice bearing permafrost should be present (Schultz and Orphal, 1978). Korteniemi et al. (2006) and Bamberg et al. (2014) define exemplary mechanisms such as intrusive volcanism, subsurface ice, groundwater migration, near surface tensile stresses, and tectonics as possible formation mechanisms for FFCs on Mars.

In comparison, FFC on Ceres share a lot of similarities with FFC on the Moon and Mars. Characteristics such as radial, concentric and polygonal fractures, flat crater floors or moat structures aspect for formation mechanisms that are similar to those described above. Pitted fracture systems like in Dantu crater indicate the influence of volatile components in the subsurface. Fractures formed by intrusions that cause uplifts are because of the morphological pattern also a good explanation, although, magmatic intrusions are not (e.g., Buczkowski et al., 2018; von der Gathen et al., 2016). Another similarity is that such floor-fractured craters are also much shallower than pristine craters of similar size or even shallower as Buczkowski et al. (2018) described comparable to the findings on the Moon.

Floor-fractured craters on Venus on the other hand are relatively rare and show an elevation dependency (Wichman, 1994; Wichman and Schultz, 1992). On this planetary body, floor fractures often occur in form of concentric failures of the crater floor, in some cases transected by wrinkle ridges and/or radial/polygonal cracks. The crater floor and outer moat shows a relative smooth surface (Wichman and Schultz, 1995b). Regional tectonism and volcanism are the mechanisms discussed to affect the crater morphologies and origin of fractures (Head et al., 2009; Wichman and Schultz, 1995b). In addition, high temperatures on the surface can favor topographic relaxation, although, Grimm and Solomon (1988) described this process as negligible and depicted the igneous intrusion model as more likely on Venus (Wichman and Schultz, 1995b). Crustal composition and surface gravity portend to two different modification possibilities. First, the crater-centered intrusions and second the crater-filling volcanism. Both mechanisms are more likely for Venus than the Moon and especially Ceres.

Due to the low resolution it is not quite clear if there are floor-fractured craters on Mercury at all (Korteniemi et al., 2006). Nevertheless, these potential FFC show evidence of intrusive activity in the planet's crust or an extrusive volcanic origin, comparable to those on Venus (Greeley, 2013; Head et al., 2009).

Floor fractured craters on icy satellites, such as Enceladus, are relatively rare. This can be explained by the rapid viscous creep of ice (Johnson and McGetchin, 1973) and the fact that small fractures would freeze relatively quickly at deep surface temperatures (Elder et al., 2012). A fracture of about 5 cm for instance would freeze in a few minutes. The process would be accelerated by possible warm ice in the underground (Roberts and Stickle, 2017). Formation mechanisms comparable to Venus, Mercury or the icy satellites could be negligible for FFC on Ceres because of the differences in surface

conditions and morphological fracture pattern.

5 Conclusion

Our study, which is mainly based on photo-geologic structural mapping, leads to following main findings: In case of Ceres' FFC the length, width and strike of the fractures vary for each crater and point to independent formation mechanisms. We suggest that the variety in length, width and orientation could denote a variety in the surface and underground conditions and composition and indicate local brittle material components. Parallel and wide fractures suggest a high anisotropy of the material, while fracture cluster and networks reduce the same.

The density map and rose histograms indicate that the main formation mechanism of the floor fractures should not be the impact process itself. Fracture patterns and pit ends of fractures rather point out formation mechanisms comparable to those on the Moon and Mars, although, an uprising of magma is unlikely and the process of relaxation not crucial in case of Ceres (Buczkowski et al., 2018; Hiesinger et al., 2016; von der Gathen et al., 2016).

Based on these investigations we derivate four main hypotheses for the formation mechanism of the FFCs on Ceres: (1) tear-off edges in case of slumping of the crater wall, (2) cooling melting processes that lead to sinkage of the crater floor, (3) degassing, and/or (4) tectonic interactions. The fourth mechanism also comprises up-doming of material for instance beneath Occator crater.

6 Acknowledgments

We thank the Dawn team for the development, cruise, orbital insertion, and operations of the Dawn spacecraft at Ceres. Portions of this work were performed at the DLR Institute of Planetary Research, at the Jet Propulsion Laboratory (JPL) under contract with NASA, as well as the German Aerospace Center (DLR). Dawn data are archived with the NASA Planetary Data System https://pds-smallbodies.astro.umd.edu/.

References

Ammannito, E., DeSanctis, M.C., Ciarniello, M., Frigeri, A., Carrozzo, F.G., Combe, J.-P., Ehlmann, B.L., Marchi, S., McSween, H.Y., Raponi, A., Toplis, M.J., Tosi, F., Castillo-Rogez, J.C., Capaccioni, F., Capria, M.T., Fonte, S., Giardino, M., Jaumann, R., Longobardo, A., Joy, S.P., Magni, G., McCord, T.B., McFadden, L.A., Palomba, E., Pieters, C.M., Polanskey, C.A., Rayman, M.D., Raymond, C.A., Schenk, P.M., Zambon, F., Russell, C.T., 2016. Distribution of phyllosilicates on the surface of Ceres. Science 353.

Bamberg, M., Jaumann, R., Asche, H., Kneissl, T., Michael, G.G., 2014. Floor-Fractured Craters on Mars – Observations and Origin. Planetary and Space Science 98, 146-162.

Boyce, J.M., Wilson, L., Mouginis-Mark, P.J., Hamilton, C.W., Tornabene, L.L., 2012. Origin of small pits in martian impact craters. Icarus 221, 262-275.

Buczkowski, D.L., Schmidt, B.E., Williams, D.A., Mest, S.C., Scully, J.E.C., Ermakov, A.I., Preusker, F., Schenk, P., Otto, K.A., Hiesinger, H., O'Brien, D., Marchi, S., Sizemore, H., Hughson, K., Chilton, H., Bland, M., Byrne, S., Schorghofer, N., Platz, T., Jaumann, R., Roatsch, T., Sykes, M.V., Nathues, A., De Sanctis, M.C., Raymond, C.A., Russell, C.T., 2016. The geomorphology of Ceres. Science 353.

Buczkowski, D.L., Sizemore, H.G., Bland, M.T., Scully, J.E.C., Quick, L.C., Hughson, K.H.G., Park, R.S., Preusker, F., Raymond, C.A., Russell, C.T., 2018. Floor-Fractured Craters on Ceres and Implications for Interior Processes. 123, 3188-3204.

Castillo-Rogez, J.C., McCord, T.B., 2010. Ceres' evolution and present state constrained by shape data. Icarus 205, 443-459.

Collins, G.S., Melosh, H.J., Ivanov, B.A., 2004. Modeling damage and deformation in impact simulations. Meteoritics and Planetary Science 39, 217-231.

Combe, J.-P., McCord, T.B., Tosi, F., Ammannito, E., Carrozzo, F.G., De Sanctis, M.C., Raponi, A., Byrne, S., Landis, M.E., Hughson, K.H.G., Raymond, C.A., Russell, C.T., 2016. Detection of local H2O exposed at the surface of Ceres. Science 353.

De Sanctis, M.C., Ammannito, E., Raponi, A., Marchi, S., McCord, T.B., McSween, H.Y., Capaccioni, F., Capria, M.T., Carrozzo, F.G., Ciarniello, M., Longobardo, A., Tosi, F., Fonte, S., Formisano, M., Frigeri, A., Giardino, M., Magni, G., Palomba, E., Turrini, D., Zambon, F., Combe, J.-P., Feldman, W., Jaumann, R., McFadden, L.A., Pieters, C.M., Prettyman, T., Toplis, M., Raymond, C.A., Russell, C.T., 2015. Ammoniated phyllosilicates with a likely outer Solar System origin on (1) Ceres. Nature 528, 241-244.

De Sanctis, M.C., Coradini, A., Ammannito, E., Filacchione, G., Capria, M.T., Fonte, S., Magni, G.,

Barbis, A., Bini, A., Dami, M., Ficai-Veltroni, I., Preti, G., 2011. The VIR Spectrometer. Space Science Reviews 163, 329-369.

Denevi, B.W., Blewett, D.T., Buczkowski, D.L., Capaccioni, F., Capria, M.T., De Sanctis, M.C., Garry, W.B., Gaskell, R.W., Le Corre, L., Li, J.-Y., Marchi, S., McCoy, T.J., Nathues, A., O'Brien, D.P., Petro, N.E., Pieters, C.M., Preusker, F., Raymond, C.A., Reddy, V., Russell, C.T., Schenk, P., Scully, J.E.C., Sunshine, J.M., Tosi, F., Williams, D.A., Wyrick, D., 2012. Pitted terrain on Vesta and implications for the presence of volatiles. Science 338, 246-249.

Dombard, A.J., Gillis, J.J., 2001. Testing the viability of topographic relaxation as a mechanism for the formation of lunar floor-fractured craters. 106, 27901-27909.

Durney, D.W., 1973. Incremental strains measured by syntectonic crystal growths. Gravity and tectonics, 67-96.

Elder, C.M., Bray, V.J., Melosh, H.J., 2012. The theoretical plausibility of central pit crater formation via melt drainage. Icarus 221, 831-843.

Engelder, T., 1987. Joints and Shear Fractures in Rock, In: Atkinson, B.K. (Ed.), Fracture Mechanics of Rock, pp. 27-69.

Greeley, R., 2013. Mercury, In: Greeley, R. (Ed.), Introduction to Planetary Geomorphology. Cambridge University Press, Cambridge, pp. 91-105.

Grimm, R.E., Solomon, S.C., 1988. Viscous relaxation of impact crater relief on Venus: Constraints on crustal thickness and thermal gradient. 93, 11911-11929.

Günzel, F.K., 2008. Shear Strength of Ice-Filled Rock Joints. Proceedings of the 9th International Conference on Permafrost.

Hall, J.L., Solomon, S.C., Head, J.W., 1981. Lunar floor-fractured craters: Evidence for viscous relaxation of crater topography. 86, 9537-9552.

Head, J.W., Murchie, S.L., Prockter, L.M., Solomon, S.C., Chapman, C.R., Strom, R.G., Watters, T.R., Blewett, D.T., Gillis-Davis, J.J., Fassett, C.I., Dickson, J.L., Morgan, G.A., Kerber, L., 2009. Volcanism on Mercury: Evidence from the first MESSENGER flyby for extrusive and explosive activity and the volcanic origin of plains. Earth and Planetary Science Letters 285, 227-242.

Healy, D., Rizzo, R.E., Cornwell, D.G., Farrell, N.J.C., Watkins, H., Timms, N.E., Gomez-Rivas, E., Smith, M., 2017. FracPaQ: A MATLAB™ toolbox for the quantification of fracture patterns. Journal of Structural Geology 95, 1-16.

Hiesinger, H., Marchi, S., Schmedemann, N., Schenk, P., Pasckert, J.H., Neesemann, A., O'Brien, D.P., Kneissl, T., Ermakov, A.I., Fu, R.R., Bland, M.T., Nathues, A., Platz, T., Williams, D.A., Jaumann, R., Castillo-Rogez, J.C., Ruesch, O., Schmidt, B., Park, R.S., Preusker, F., Buczkowski, D.L., Russel, C.T., Raymond, C.A., 2016. Cratering on Ceres: Implications for its crust and evolution. Science 353.

Johnson, T.V., McGetchin, T.R., 1973. Topography on satellite surfaces and the shape of asteroids. Icarus 18, 612-620.

Jozwiak, L.M., Head, J.W., Wilson, L., 2015. Lunar floor-fractured craters as magmatic intrusions: Geometry, modes of emplacement, associated tectonic and volcanic features, and implications for gravity anomalies. Icarus 248, 424-447.

Jozwiak, L.M., Head, J.W., Zuber, M.T., Smith, D.E., Neumann, G.A., 2012. Lunar floor-fractured craters: Classification, distribution, origin and implications for magmatism and shallow crustal

694 structure. Journal of Geophysical Research (Planets) 117.

695 Korteniemi, J., Aittola, M., Öhman, T., Raitala, J., 2006. Floor-fractured craters on the terrestrial
696 planets–The martian perspective. Proceedings of the First International Conference on Impact
697 Cratering in the Solar System, Eur. Space Agency Spec. Publ., SP-612.

698 Krautblatter, M., Funk, D., Günzel, F.K., 2013. Why permafrost rocks become unstable: a rock–ice-
699 mechanical model in time and space. 38, 876-887.

700 Krönert, W., Böhm, A., 1980. Temperaturwechselverhalten tonerdereicher feuerfester Steine im
701 Bereich hoher Temperaturen. Institut für Gesteinshüttenkunde Rhein.-Westf. Techn. Hochschule
702 Aachen, Westdeutscher Verlag.

703 McCord, T.B., Sotin, C., 2005. Ceres: Evolution and current state. Journal of Geophysical Research
704 (Planets) 110, 5009.

705 Moore, C.H., 1989. The Classification and Nature of Carbonate Porosity, In: Moore, C.H. (Ed.),
706 Developments in Sedimentology. Elsevier, pp. 21-41.

707 Moore, D.E., Lockner, D.A., 1995. The role of microcracking in shear-fracture propagation in granite.
708 Journal of Structural Geology 17, 95-114.

709 Nelson, S.A., 2015. Deformation of rocks, EENS 1110,
710 http://www.tulane.edu/~sanelson/eens1110/deform.htm.

711 Nemec, W., 1988. The shape of the rose. Sedimentary Geology 59, 149-152.

712 Otto, K.A., Jaumann, R., Krohn, K., Buczkowski, D.L., von der Gathen, I., Kersten, E., Mest, S.C.,
713 Naß, A., Neesemann, A., Preusker, F., Roatsch, T., Schröder, S.E., Schulzeck, F., Scully, J.E.C.,
714 Stephan, K., Wagner, R., Williams, D.A., Raymond, C.A., Russell, C.T., 2016. Characteristics of
715 Polygonal Craters on (1) Ceres, EGU General Assembly Conference Abstracts, p. 8737.

716 Park, R.S., Konopliv, A.S., Bills, B.G., Rambaux, N., Castillo-Rogez, J.C., Raymond, C.A., Vaughan,
717 A.T., Ermakov, A.I., Zuber, M.T., Fu, R.R., Toplis, M.J., Russell, C.T., Nathues, A., Preusker, F.,
718 2016. A partially differentiated interior for (1) Ceres deduced from its gravity field and shape. Nature
719 537, 515-517.

720 Pollard, D.D., Segall, P., Delaney, P.T., 1982. Formation and interpretation of dilatant echelon cracks.
721 GSA Bulletin 93, 1291-1303.

722 Prettyman, T.H., Feldman, W.C., McSween, H.Y., Dingler, R.D., Enemark, D.C., Patrick, D.E.,
723 Storms, S.A., Hendricks, J.S., Morgenthaler, J.P., Pitman, K.M., Reedy, R.C., 2011. Dawn's Gamma
724 Ray and Neutron Detector. Space Science Reviews 163, 371-459.

725 Preusker, F., Scholten, F., Matz, K.-D., Elgner, S., Jaumann, R., Roatsch, T., Joy, S.P., Polanskey,
726 C.A., Raymond, C.A., Russell, C.T., 2016. Dawn at Ceres — Shape Model and Rotational State,
727 Lunar and Planetary Science Conference, p. 1954.

728 Priest, S.D., Hudson, J.A., 1981. Estimation of discontinuity spacing and trace length using scanline
729 surveys. International Journal of Rock Mechanics and Mining Sciences & Geomechanics Abstracts 18,
730 183-197.

731 Roatsch, T., Kersten, E., Matz, K.D., Preusker, F., Scholten, F., Jaumann, R., Raymond, C.A., Russell,
732 C.T., 2016. High-resolution Ceres High Altitude Mapping Orbit atlas derived from Dawn Framing
733 Camera images. Planetary and Space Science 140, 74-79.

734 Roatsch, T., Kersten, E., Matz, K.D., Preusker, F., Scholten, F., Jaumann, R., Raymond, C.A., Russell,

C.T., 2017. High-resolution Ceres Low Altitude Mapping Orbit Atlas derived from Dawn Framing Camera images. Planetary and Space Science 140, 74-79.

Roberts, J.H., Stickle, A.M., 2017. Break the World's Shell: An Impact on Enceladus: Bringing the Ocean to the Surface, LPSC The Woodlands, p. 1955.

Rodríguez, J.A.P., Sasaki, S., Dohm, J.M., Tanaka, K.L., Strom, B., Kargel, J., Kuzmin, R., Miyamoto, H., Spray, J.G., Fairén, A.G., Komatsu, G., Kurita, K., Baker, V., 2005. Control of impact crater fracture systems on subsurface hydrology, ground subsidence, and collapse, Mars. 110.

Rouleau, A., Gale, J.E., 1985. Statistical characterization of the fracture system in the Stripa granite, Sweden. International Journal of Rock Mechanics and Mining Sciences & Geomechanics Abstracts 22, 353-367.

Ruesch, O., Platz, T., Schenk, P., McFadden, L.A., Castillo-Rogez, J.C., Quick, L.C., Byrne, S., Preusker, F., O'Brien, D.P., Schmedemann, N., Williams, D.A., Li, J.-Y., Bland, M.T., Hiesinger, H., Kneissl, T., Neesemann, A., Schaefer, M., Pasckert, J.H., Schmidt, B.E., Buczkowski, D.L., Sykes, M.V., Nathues, A., Roatsch, T., Hoffmann, M., Raymond, C.A., Russell, C.T., 2016. Cryovolcanism on Ceres. Science 353.

Russell, C.T., Raymond, C.A., 2011. The Dawn mission to Vesta and Ceres. Space Science Reviews 163, 3-23.

Russell, C.T., Raymond, C.A., Ammannito, E., Buczkowski, D.L., De Sanctis, M.C., Hiesinger, H., Jaumann, R., Konopliv, A.S., McSween, H.Y., Nathues, A., Park, R.S., Pieters, C.M., Prettyman, T.H., McCord, T.B., McFadden, L.A., Mottola, S., Zuber, M.T., Joy, S.P., Polanskey, C., Rayman, M.D., Castillo-Rogez, J.C., Chi, P.J., Combe, J.P., Ermakov, A., Fu, R.R., Hoffmann, M., Jia, Y.D., King, S.D., Lawrence, D.J., Li, J.-Y., Marchi, S., Preusker, F., Roatsch, T., Ruesch, O., Schenk, P., Villarreal, M.N., Yamashita, N., 2016. Dawn arrives at Ceres: Exploration of a small, volatile-rich world. Science 353, 1008-1010.

Salguero-Hernández, E., Fucugauchi, J., Ramírez-Cruz, L., 2010. Fracturing and deformation in the Chicxulub crater Complex trace analysis of instantaneous seismic attributes. Revista mexicana de ciencias geológicas, ISSN 1026-8774, Vol. 27, Nº. 1, 2010, pags. 175-184 27.

Sato, H., Kurita, K., Baratoux, D., 2010. The formation of floor-fractured craters in Xanthe Terra. Icarus 207, 248-264.

Schultz, P.H., 1976. Floor-fractured lunar craters. Moon 15, 241-273.

Schultz, P.H., 1978. Martian intrusions: Possible sites and implications. 5, 457-460.

Schultz, P.H., Orphal, D.L., 1978. Floor-Fractured Craters on the Moon and Mars. Meteoritics 13, 622.

Scully, J., Buczkowski, D., King, S., Castillo-Rogez, J., Schmedemann, N., O'Brien, D., Raymond, C., Marchi, S., Russell, C., Mitri, G., Bland, M., 2016. Geologic Mapping of Fractures and Secondary Crater Chains Uncovers.

Sierks, H., Keller, H.U., Jaumann, R., Michalik, H., Behnke, T., Bubenhagen, F., Büttner, I., Carsenty, U., Christensen, U., Enge, R., Fiethe, B., Gutiérrez Marqués, P., Hartwig, H., Krüger, H., Kühne, W., Maue, T., Mottola, S., Nathues, A., Reiche, K.-U., Richards, M.L., Roatsch, T., Schröder, S.E., Szemerey, I., Tschentscher, M., 2011. The Dawn Framing Camera. Space Science Reviews 163, 263-327.

Singhal, B.B.S., Gupta, R.P., 1999. Fractures and discontinuities, In: Singhal, B.B.S., Gupta, R.P. (Eds.), Applied Hydrogeology of Fractured Rocks. Springer Netherlands, Dordrecht, pp. 13-35.

778 Sizemore, H.G., Platz, T., Schorghofer, N., Prettyman, T.H., De Sanctis, M.C., Crown, D.A.,
779 Schmedemann, N., Neesemann, A., Kneissl, T., Marchi, S., Schenk, P.M., Bland, M.T., Schmidt, B.E.,
780 Hughson, K.H.G., Tosi, F., Zambon, F., Mest, S.C., Yingst, R.A., Williams, D.A., Russell, C.T.,
781 Raymond, C.A., 2017. Pitted terrains on (1) Ceres and implications for shallow subsurface volatile
782 distribution. Geophysical Research Letters 44, 6570-6578.

783 von der Gathen, I., Jaumann, R., Krohn, K., Buczkowski, D.L., Elgner, S., Kersten, E., Matz, K.D.,
784 Nass, A., Otto, K., Preusker, F., Roatsch, T., Schröder, S.E., Schulzeck, F., Stephan, K., Wagner, R.,
785 De Sanctis, M.C., Schenk, P., Scully, J.E.C., Williams, D.A., Raymond, C.A., Russell, C.T., 2016.
786 Deformational Features on Ceres' Surface Compared to Other Planetary Bodies, Lunar and Planetary
787 Science Conference, p. 1961.

788 Wichman, R.W., 1994. Dark-Floored Crater Elevations on Venus: Implications for Crater-centered
789 Volcanism, Lunar and Planetary Science Conference, p. 1489.

790 Wichman, R.W., Schultz, P.H., 1992. Floor-fractured Crater Models for Igneous Crater Modification
791 on Venus, International Colloquium on Venus, p. 131.

792 Wichman, R.W., Schultz, P.H., 1995a. Floor-fractured craters in Mare Smythii and west of Oceanus
793 Procellarum: Implications of Crater Modification by Viscous Relaxation and Igneous Intrusion
794 Models. Journal of Geophysical Research 100, 21201-21218.

795 Wichman, R.W., Schultz, P.H., 1995b. Floor-fractured impact craters on Venus: Implications for
796 igneous crater modification and local magmatism. Journal of Geophysical Research 100, 3233-3244.
797